CrossMark

Optimized design of moth eye antireflection structure for organic photovoltaics

Shigeru Kubota, Kensaku Kanomata, Bashir Ahmmad, Jun Mizuno, Fumihiko Hirose

Abstract To improve the power conversion efficacy of organic photovoltaics (OPVs), it is required to design antireflection structures that could realize efficient and broadband light trapping. In this article, we perform global optimization of the textured pattern of moth eye antireflection surfaces to maximize the short-circuit current density (J_{SC}) of OPVs with a poly(3-hexylthiophene) (P3HT) and [6,6]-phenyl-C_{61}-butyric acid methyl ester (PCBM)-based bulk heterojunction. We introduce an optimization algorithm consisting of two steps: in the first step, the simple grid search is conducted to roughly estimate a globally optimal solution, while in the second step, the Hooke and Jeeves pattern search is executed to refine the solution. By combining the optimization algorithm with the optical simulation based on the finite-difference time-domain method, we find the optimal period and height of moth eye array with which the level of J_{SC} can be increased by 9.05% in the P3HT:PCBM-based organic solar cell. We also demonstrate that the optimized moth eye structure can significantly modify the light path at a long wavelength range to strengthen the electric field intensity and enhance energy absorption within the active layer.

Keywords Organic solar cell, Moth eye, Optimization, FDTD

S. Kubota (✉), K. Kanomata, B. Ahmmad, F. Hirose
Graduate School of Science and Engineering, Yamagata University, 4-3-16 Jonan, Yonezawa, Yamagata 992-8510, Japan
e-mail: kubota@yz.yamagata-u.ac.jp

S. Kubota, B. Ahmmad, F. Hirose
CREST, Japan Science and Technology Agency, 4-3-16 Jonan, Yonezawa, Yamagata 992-8510, Japan

K. Kanomata
Japan Society for the Promotion of Science, 5-3-1 Kojimachi, Chiyoda-ku, Tokyo 102-0083, Japan

J. Mizuno
Research Organization for Nano and Life Innovation, Waseda University, 513 Wasedatsurumaki-cho, Shinjyuku-ku, Tokyo 162-0041, Japan

Introduction

Organic photovoltaics (OPVs) have recently been proposed as a key for energy supply, because they could be cost-effective, flexible, and lightweight power generation devices in the near future.[1–4] The power conversion efficiencies of OPVs have been considerably increasing in the last decade,[5] although further improvement will be required for large-scale commercialization. A widely studied OPV device contains a thin photoactive layer which is sandwiched by a transparent front and a highly reflective back electrode. Generally, the active layer should be as thin as ~100 nm, since a low mobility of organic semiconductors makes it difficult to extract charge carrier from them.[6–8] To enhance light absorption and attain higher conversion efficacy, it is quite important to develop an efficient antireflection structure (ARS) that allows for light trapping in such thin active layer.

Currently, the most widely used technique for antireflection of solar cells is the multilayer interference coating, in which dielectric materials with different refractive indexes are deposited in one dimension.[9] This structure can reduce the effect of mismatch in optical admittance between materials to suppress light reflection, but the availability of materials with suitable refractive indexes ultimately limits the effectiveness of this approach.[10] For more efficient antireflection, recent studies are focusing on the moth eye texturing, a nanostructure inspired by the corneal surface of moth's eyes.[10–15] In the moth eye coating, the device

surface is covered with two-dimensional cone array with a period and height of several hundred nanometers. This nanostructure functions to make a gradual change in refractive index from that of the incident medium to the device, producing broadband antireflection effect. A recent experimental study showed that by applying moth eye coating to the OPVs, the power conversion efficacy was increased by 2.5–3% for a wide range of incident angles.[15]

However, recent studies also suggest that the antireflective performance of moth eye texture highly depends on the geometric pattern of cone array.[10,14,16] The theoretical study by Deinega et al.[14] showed that, for silicon moth eye surfaces, the minimal reflectance is achieved when the height of cone array is sufficiently large and its period takes an adequate value within a quite restricted range. Simulations by Boden and Bagnall[10] also showed that the reflectance is given by a complicated function of the wavelength of light, and the period and height of silicon moth eye array. These studies strongly suggest that the numerical optimization of geometric parameters of cone array is necessary to bring out a full performance of moth eye texture. However, the global optimization of textured pattern is quite difficult, since the optical simulation of nanostructure generally requires fine meshes and small time steps for stable computation, resulting in a high computational cost.[17] In addition, previous simulation studies on the surface nanotexture mainly addressed the cases of silicon substrate, and thus, the textured pattern adequate for OPVs is largely unclear. A recent study in our group[16] executed numerical optimization of a hybrid ARS that combines moth eye texture and two-layer interference coating for application to OPVs. But, the previous study examined the inverse configuration of OPVs, in which the bottom electrode is in contact with a substrate, to reduce computational efforts. Thus, the optimization of the textured surfaces for a widely used configuration of OPVs, in which the front transparent electrode is in contact with a glass substrate,[3,5] has not yet been conducted. In the usual devices, light waves pass through a glass substrate that is much thicker than the thin film OPV cell. Since the thick substrate drastically increases the number of grid points required for the simulation, the optimization of the antireflection texture for the generally used type of OPVs necessitates extensive computational cost.[16,18]

In this study, we perform numerical optimization of the geometric feature of moth eye texture, for the widely used type of OPV devices, in which light goes through the glass substrate to enter the solar cell. To estimate the cell performance, we conduct simulations based on the finite-difference time-domain (FDTD) method,[17] which is frequently used for analyzing optical properties of nanostructure. To achieve the efficient FDTD simulations in the presence of a thick substrate, we introduce a computational algorithm for simulating incoherent addition of light in the glass substrate.[19–21] By conducting global optimization, we find the period and height of moth eye array to maximize the short-circuit current density (J_{SC}) of OPVs. In addition, we investigate the changes in the absorbed energy spectrum and electric field distribution in the active layer, which underlie the improvement in performance. These results offer an efficient and practical ARS design method to achieve broadband light trapping in the thin active layer of OPVs.

Experimental

Optical model

We numerically analyzed the effect of moth eye antireflection coating on the efficacy of OPVs. Figure 1a illustrates the structure of a thin film OPV cell in the absence of moth eye array, which serves as the reference for evaluating performance. As shown in the figure, the OPV cell is generally deposited on a glass substrate with a millimeter-order thickness. Similar to
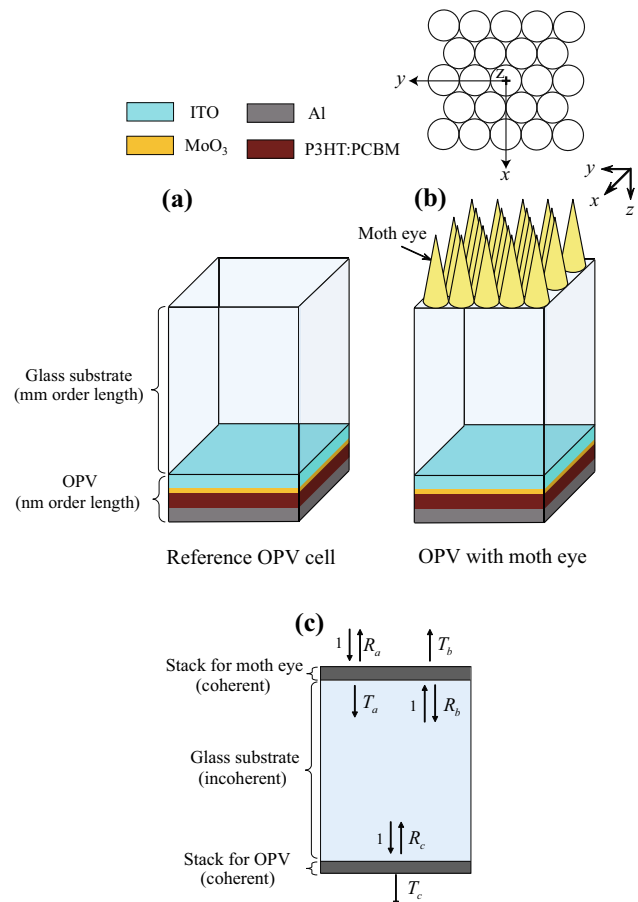
Fig. 1: Device structures for a reference OPV cell (a) and an OPV cell with moth eye texture (b). (c) In the characteristic matrix-based analysis, the device with moth eye is considered to be an assembly of a glass substrate and two multilayer stacks which represent the moth eye and OPV cell

the previous simulation,[18] the optical model in this study is assumed to contain a 5-μm-thick glass substrate, which is sufficient to provide accurate prediction of the solar cell performance (see "Results and discussion"). The examined device includes a 100-nm-thick film of poly(3-hexylthiophene) (P3HT) and [6,6]-phenyl-C_{61}-butyric acid methyl ester (PCBM) blend as the active layer, and a 7-nm MoO_3 film as the hole transporting layer.[16,19] These materials are sandwiched by a transparent 100-nm indium-doped tin oxide (ITO) layer and a 100-nm Al layer, which work as the forward and bottom electrodes, respectively.[16,19] The model for the OPV cell with moth eye coating is shown in Fig. 1b, where the cones are hexagonally arranged on the front surface of the solar cell. In the moth eye array, the base circles of two nearby cones touch each other. The geometric pattern of moth eye structure is characterized by the period L, which is the distance between the tips of adjacent cones, as well as the height H of each cone. The moth eye coat is assumed to be fabricated with organic polymer, because nanoimprint lithography (NIL) with polymeric resist is frequently used for low-cost realization of nanopatterned surfaces.[22–25] Accordingly, the refractive index of moth eye array is set to be 1.5, which is a typical value for organic polymer materials.[26]

FDTD simulation

Optical simulations with the FDTD method were performed to evaluate the level of J_{SC}. The coordinate system is illustrated in Fig. 1b, where the z-axis corresponds to the direction of propagation of incident light. We introduced the absorbing boundary conditions using the perfectly matched layer technique[17] for the upper and lower boundaries in z-direction. The FDTD simulation using unpolarized sunlight usually requires averaging of optical response obtained by the x- and y-polarized incident light.[27] However, in our optical model, due to a high symmetry of moth eye pattern, the difference in J_{SC} by applying the x- and y-polarized light is much smaller than its change obtained by the moth eye (~4–9%; Fig. 5).[16] Therefore, the results with the x-polarized incident light are shown throughout this study.

To evaluate J_{SC}, we first estimate the absorbance in the active layer from the FDTD simulation. Since the FDTD response shows strong oscillation in the presence of the thick glass substrate,[18] we remove the oscillatory component of the absorbance ("Results and discussion"). If we let $A_p(\lambda)$ be the absorbance in the active layer at wavelength λ, the number of absorbed photons, $N_p(\lambda)$, can be expressed as follows[16,19,27]:

$$N_p(\lambda) = A_p(\lambda)F(\lambda)\frac{\lambda}{hc}. \tag{1}$$

Here $F(\lambda)$ denotes the solar irradiance spectrum under AM 1.5 illumination,[28] h is Planck's constant, and c is

the velocity of light in free space. With the unit charge q_e, the number of photons is converted to the photocurrent by the following equation[16,19,27]:

$$J_{SC} = \int_0^{\lambda_g} q_e N_p(\lambda)F_{NR}(\lambda)d\lambda, \tag{2}$$

where λ_g is the wavelength corresponding to the band gap of P3HT (653 nm). $F_{NR}(\lambda)$ is the nonrecombination factor and is simply assumed to be $F_{NR}(\lambda) = 1$ for all λ.[29] In addition, we calculate the weighted reflectance as follows[30]:

$$R_w = \frac{\int_0^{\lambda_g} R(\lambda)F(\lambda)d\lambda}{\int_0^{\lambda_g} F(\lambda)d\lambda}, \tag{3}$$

where $R(\lambda)$ represents the reflectance at wavelength λ.

The optical data for the materials of MoO_3, P3HT:PCBM (1:1 by weight), Al, and glass were prepared by the measurements of spectroscopic ellipsometry (the ellipsometry data for P3HT:PCBM were plotted in Fig. 2 as an example). The optical data for ITO were taken from Hoppe et al.[31] These data were fitted by the Lorentz–Drude model,[32] which permits efficient FDTD simulations for dispersive materials.[17]

The FDTD simulations were executed by repetitively running the OptiFDTD software from a MATLAB program to conduct optimization search. To obtain a broadband response from a single FDTD simulation, the result obtained by a brief pulse of incident light was Fourier transformed at 200 frequencies, which are equally distributed from 416 to 1071 THz (corresponding to the wavelength from 280 to 720 nm).[17] The FDTD simulation of our model (Fig. 1) required ~3 h for each case on our PC equipment (Intel Core i7 3.40 GHz).
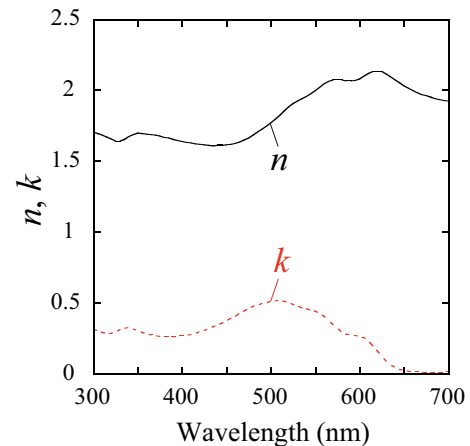
Fig. 2: Optical data of P3HT:PCBM obtained by the spectroscopic ellipsometry. The refractive index (*n*) and extinction coefficient (k) are plotted by the solid and dashed lines, respectively, as a function of wavelength

Characteristic matrix-based analysis

In order to verify the results of FDTD simulation, we also performed an analysis based on the characteristic matrix method.[9] The optical properties of moth eye texture were determined by applying the effective medium theory.[33] This theory can be generally used to describe the optical properties of nanotexture when the periodicity of the textured pattern is sufficiently small compared to the wavelength of incident light.[15] Since the moth eye texture can be described as a multilayer stack with a graded refractive index by using the effective medium theory, the OPV device with the moth eye array consists of two thin film stacks, corresponding to the moth eye and the OPV cell, and a much thicker glass substrate (Fig. 1c). Within each stack, the light is added coherently by the characteristic matrix-based formalism, whereas in the thick substrate, the addition of irradiances (not optical field amplitudes) is considered due to the loss of coherence.[19–21]

For a thin film stack (with q layers), the reflectance R and transmittance T are generally described as follows[9,19]:

$$R = \left(\frac{\eta_i B - C}{\eta_i B + C}\right)\left(\frac{\eta_i B - C}{\eta_i B + C}\right)^*, \qquad (4)$$

and

$$T = \frac{\text{Re}(\eta_e)}{\text{Re}(\eta_i)}\left(\frac{2\eta_i}{\eta_i B + C}\right)\left(\frac{2\eta_i}{\eta_i B + C}\right)^*, \qquad (5)$$

Here η_i and η_e are the optical admittances for the incident and emergent media, respectively, and B and C are obtained by

$$\begin{bmatrix} B \\ C \end{bmatrix} = M_1 M_2 \cdots M_q \begin{bmatrix} 1 \\ \eta_e \end{bmatrix}. \qquad (6)$$

The characteristic matrix M_r corresponding to the rth layer is given by

$$M_r = \begin{bmatrix} \cos \delta_r & (i \sin \delta_r)/\eta_r \\ i\eta_r \sin \delta_r & \cos \delta_r \end{bmatrix}, \qquad (7)$$

where δ_r represents the phase difference between the top and bottom of the rth layer, and η_r denotes the optical admittance for the material of the rth layer. From equations (4)–(7), the reflectance and transmittance for each multilayer stack (i.e., R_X and T_X with $X = a$, b, or c in Fig. 1c) can be obtained.

If we assume that the active layer is the pth layer in the multilayer stack for the OPV cell, the absorbance A_p in the active layer is described as follows[9,19]:

$$A_p = I_s(\psi_{p-1} - \psi_p), \qquad (8)$$

$$\psi_r = \frac{\text{Re}(B_r C_r^*)}{\text{Re}(BC^*)} \text{ for all } r, \qquad (9)$$

$$\begin{bmatrix} B_r \\ C_r \end{bmatrix} = M_{r+1} M_{r+2} \cdots M_q \begin{bmatrix} 1 \\ \eta_e \end{bmatrix}. \qquad (10)$$

Here ψ_r denotes the potential transmittance for the subassembly including the thin films from the front side to the rth layer in the stack for OPV cell. By taking into account the multiple reflection occurring at the interfaces between the substrate and the two stacks (Fig. 1c), the irradiance I_s of the light entering the multilayer stack for OPV is described as

$$I_s = \frac{T_a T_c}{\psi_t (1 - R_b R_c)}, \qquad (11)$$

where ψ_t is the potential transmittance for all the layers in the stack. R_b, R_c, T_a, and T_c are the reflectance and transmittance which are illustrated in Fig. 1c.[9] By substituting the value of A_p for each wavelength λ into equation (1) and using equation (2), the value of J_{SC} can be obtained.

Optimization algorithm

Numerical optimization of the height H and period L of moth eye array was conducted to maximize J_{SC}. The FDTD simulation of the present model takes time of the order of hours (~3 h) as mentioned above, which requires very high computational cost for optimization search. In order to efficiently search for a globally optimal solution, we used a two-step algorithm,[16] in which the methods of the simple grid search (SGS)[34,35] and the Hooke and Jeeves pattern search (PS)[34,36,37] were applied as the first and second step, respectively. The solution obtained by the first step was used as the starting search point in the second step.

The SGS is an algorithm which is the most frequently used to solve global optimization problems.[34,35] In this algorithm, a uniform grid is considered in parameter space. Then, all the points in the grid are evaluated to find an optimum solution. In the PS algorithm proposed by Hooke and Jeeves,[36] the two phases, called exploratory and pattern moves, are repeated alternately. In the exploratory move, the search point travels toward all directions in a local parameter space from the base point $\mathbf{x}_b$, which is a starting search point of the exploratory move. Let $\mathbf{x}_n$ be a point giving the best value of objective function within the points visited in the current exploratory move. In the pattern move following the exploratory move, the base point is shifted by a relatively long distance such that $\mathbf{x}_b \leftarrow \mathbf{x}_n + (\mathbf{x}_n - \mathbf{x}_p)$, where $\mathbf{x}_p$ represents the point corresponding to the best objec-

tive function value visited in the previous iteration. $\mathbf{x}_n - \mathbf{x}_p$ is a vector giving the prediction of the best search direction at the present time. The new base point is employed in the exploratory move for the next round of iteration. The aim of the pattern move is to accelerate the optimization search based on the information regarding the objective function obtained in the past. The PS algorithm is finished when the base point arrives at an optimal solution at which the exploratory move cannot improve the objective function value.

The purpose of SGS is to obtain rough estimation of the globally optimal solution, whereas the purpose of PS is to refine the solution obtained by SGS. Thus, the step size used in PS ($\Delta L = 16$ nm and $\Delta H = 1$ nm) is set to be much smaller than that used in SGS ($\Delta L = 96$ nm and $\Delta H = 100$ nm) for each parameter.

Results and discussion

FDTD simulation in the presence of thick glass substrate

We performed optical analysis using the FDTD method to evaluate J_{SC} of the OPV device (Fig. 1). In the FDTD simulation with a thick glass substrate, the interference of light waves reflecting at the front and back sides of the substrate produces strong oscillatory response as a function of wavelength.[18] The black solid line in Fig. 3 shows an example of the oscillation occurring in the absorbance in the active layer. Such oscillatory response is 'artificial' in the sense that it does not occur in the actual device. This is
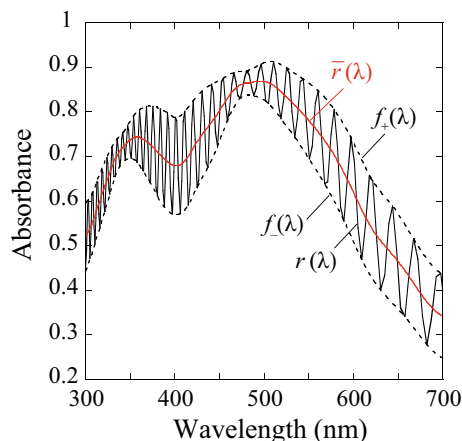

Fig. 3: An example of the artificial interference effect in the FDTD response due to a thick glass substrate. Black solid line: the spectrum of absorbance in the active layer which is directly obtained by the FDTD simulation ($r(\lambda)$). Black dashed lines: the upper and lower envelopes of the absorbance spectrum ($f_+(\lambda)$ and $f_-(\lambda)$, respectively). Red line: the absorbance spectrum in which the artificial interference effect has been removed by the proposed method ($\bar{r}(\lambda)$) (Color figure online)

because, in the substrate much thicker than the wavelength, the coherence is lost and the addition of irradiances takes place, as mentioned above.[20,21]

To remove this artificial interference effect emerging in FDTD simulations, we propose a simple but efficient method as follows. Let us consider $r(\lambda)$ to be the oscillatory response as function of wavelength λ, which is directly obtained by FDTD simulation (Fig. 3, black solid line). The local peaks of oscillation represent the states where the value of r is maximally strengthened by the interference of light passing through the substrate, whereas the local troughs of oscillation represent the states where the value of r is maximally weakened by the interference. Therefore, it can be readily expected that the averaging between the states corresponding to the peaks and troughs leads to the cancellation of the artificial interference effect. To do this, we generate the upper (lower) envelope of $r(\lambda)$, denoted as $f_+(\lambda)$ ($f_-(\lambda)$), by plotting the spline curves connecting the peaks (troughs) of oscillation (Fig. 3, dashed lines), and then take an average between the envelops $\bar{r}(\lambda) = (f_+(\lambda) + f_-(\lambda))/2$ (Fig. 3, red line) (the detailed method for obtaining $\bar{r}(\lambda)$ is given in "Appendix: Method for removing artificial interference effect from FDTD response").

In order to ensure the validity of the proposed method, we compared the results obtained by this method with those obtained by the characteristic matrix-based analysis, in which the incoherent addition of light within the thick substrate is rigorously considered (see "Experimental"). In Fig. 4a, we plotted the spectra of the absorbance in the active layer acquired by the two different methods for the cases with and without the moth eye array. Here, the period of moth eye was set to be 32 nm, since the application of the effective medium theory[33] to the textured pattern requires that its periodicity is small compared to the wavelength,[15] as mentioned above. As shown in the figure, the absorbance spectrum obtained by these methods agree quite well in both the presence and absence of moth eye. Furthermore, in Fig. 4b, we plotted the values of J_{SC} obtained by the two methods as function of the height H of moth eye array. We also plotted in the same figure the relative difference in J_{SC} estimated by the different methods, which is defined as $\delta_{Jsc} = [(J_{SC}$ obtained by FDTD with the proposed method)/(J_{SC} obtained by the characteristic matrix-based analysis) $- 1] \times 100$ (%) (Fig. 4b, red). The result shows that the value of $|\delta_{Jsc}|$ is less than 0.5% for all H values. The fact that the value of $|\delta_{Jsc}|$ is much smaller than the increase rate of J_{SC} that can be attained by the moth eye antireflection (9.05%; see below) suggests the validity of applying the proposed method to the current optimization problem. In addition, we found that the accuracy of this method and its robustness against parameter variation are significantly higher than the other conceivable approaches to remove the artificial interference, such as the simple averaging or low-pass filtering of the FDTD response.[38] The absorbance in the active layer acquired
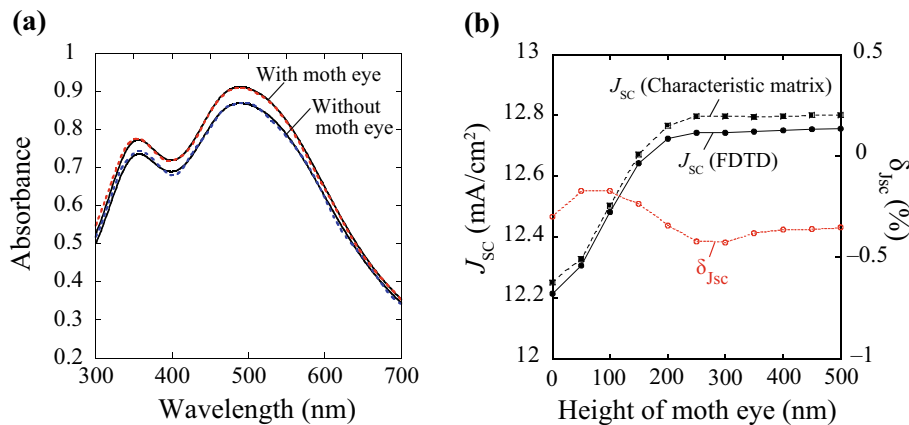
Fig. 4: Comparison between the results obtained by applying the proposed method to the FDTD response and those obtained by the characteristic matrix-based analysis. (a) Colored dashed lines: the spectra of absorbance in the active layer which are estimated by removing the artificial interference effect from the results of FDTD simulation. The red and blue dashed lines correspond to the cases with and without the moth eye texture, respectively. Black solid lines: the absorbance spectra obtained by the characteristic matrix-based analysis for both the cases with and without the moth eye. The moth eye array used here has the period of 32 nm and the height of 300 nm. (b) Black lines: the functions of the J_{SC} value vs the height of moth eye, which are obtained by the FDTD simulation with the proposed method (solid) and by the characteristic matrix-based method (dashed). Red line: the relative difference in J_{SC} estimated by the two different methods, which is defined as $\delta_{Jsc} = [(J_{SC}$ obtained by FDTD with the proposed method)/(J_{SC} obtained by the characteristic matrix-based analysis) $- 1] \times 100$ (%) (Color figure online)

by the proposed method is used to evaluate J_{SC} in the following section.
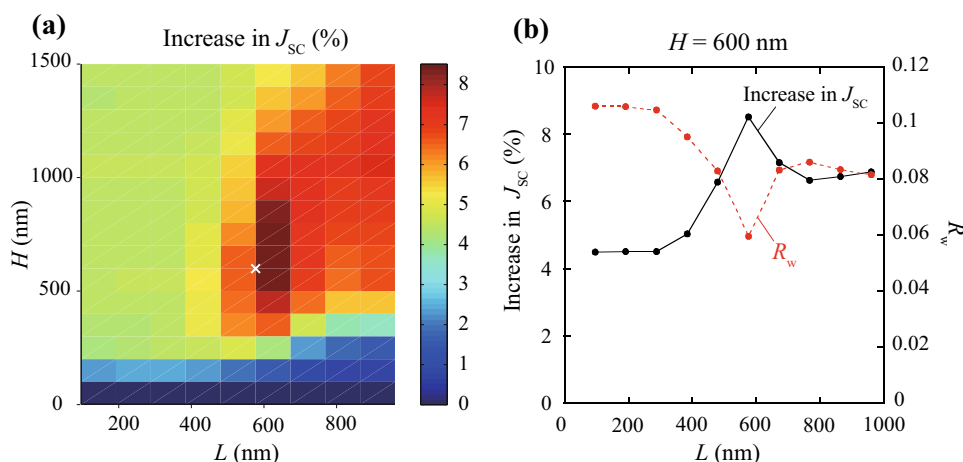
Optimization of moth eye texture

We performed numerical optimization of the parameters characterizing the moth eye texture (period L and height H) according to the two-step algorithm. Figure 5a shows the increase rate of J_{SC} due to the moth eye coating, which is obtained by the SGS in the first step, as a function of L and H. The level of J_{SC} tends to be high in the upper-right area in the figure, where both the values of L and H are relatively large. The increase in J_{SC} is correlated with the decrease in the weighted reflectance R_w (Fig. 5b), implying that the enhanced performance is attributable to the improved light trapping. The optimal solution obtained by SGS is $L = 576$ nm and $H = 600$ nm, which is represented by the x-mark in Fig. 5a. The corresponding J_{SC} value is 13.25 mA/cm², which is 8.52% higher than the J_{SC} value for the reference OPV cell (Fig. 1a; $J_{SC} = 12.21$ mA/cm²). To refine the solution, we next conducted local optimization using the PS algorithm in the second step. The starting search point for PS was set to be the solution obtained by SGS. We found the final optimal solution for moth eye texture given by $L = 592$ nm and $H = 601$ nm. The J_{SC} value for the optimal solution is 13.31 mA/cm², which is higher than that of the reference cell by 9.05%.

In the previously published study by our group,[16] the numerical optimization of the moth eye texture was conducted for application to an OPV with inverted configuration, in which a substrate is at the back side of the device and the light does not pass through the substrate. The previous study showed that the optimal height of cone array is 901 nm, which is much greater than that of the present study (601 nm), although the optimal periodicity is the same for both studies. Therefore, we can find that the addition of the glass substrate in the front side of OPV cells (Fig. 1) has an effect of significantly decreasing the height of cone array used in the optimal configuration.

Widely used moth eye textures have the periodicity of less than 300 nm,[23,39,40] which is much smaller than the optimal period found in this study (592 nm). Our findings also suggest that for such smaller period of moth eye, the increase rate of J_{SC} is as low as ~4% (Fig. 5), even if its height is sufficiently large, and this value is much lower than the optimal value (9.05%). These results suggest that it is important to select a longer period of moth eye to reach its full potential for OPVs.

To elucidate the reason why the moth eye with a longer period is effective in enhancing the performance, we examined how the spectrum of energy absorbed in the active layer is altered by the moth eye period (Fig. 6). In Fig. 6a, the blue and red lines show the spectra for the cases of applying the moth eye with the optimized configuration ($L = 592$ nm, $H = 601$ nm) and with a smaller L value ($L = 240$ nm, $H = 601$ nm), respectively. Here, we also plotted the absorbed energy spectrum for the reference OPV cell (black line) and the AM1.5 solar irradiance spectrum (green line), for comparison. The figure shows that the light absorption significantly weakened

Fig. 5: Results obtained by the simple grid search (SGS). (a) The increase rate of J_{SC}, compared to that of the reference cell, is plotted as a function of the period L and height H of moth eye texture. The x-mark denotes the point corresponding to the maximum J_{SC} value. (b) The increase rate of J_{SC} (black solid) and the weighted reflectance R_w (red dashed) are plotted as a function of L for $H = 600$ nm (Color figure online)
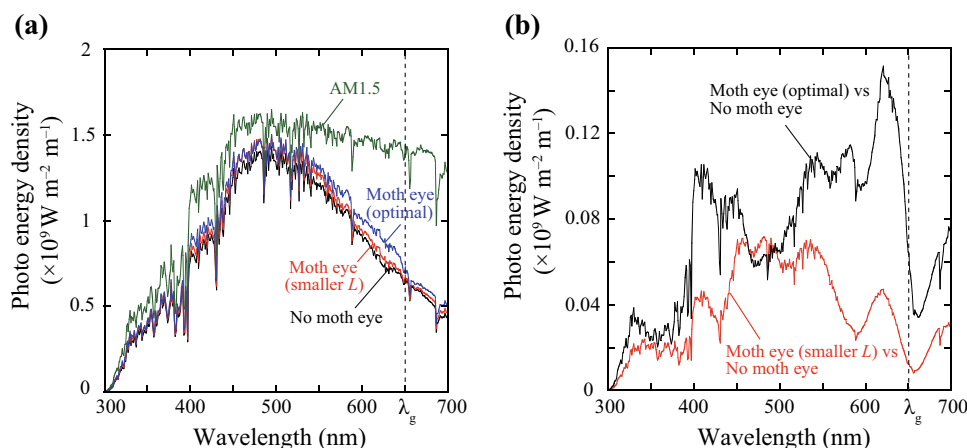

Fig. 6: Changes in the spectrum of absorption energy in the active layer generated by the moth eye array. (a) Blue and red lines: the absorption spectra for the cases of applying the optimal moth eye structure ($L = 592$ nm and $H = 601$ nm) (blue) and the moth eye with a smaller period ($L = 240$ nm and $H = 601$ nm) (red). Black line: the absorption spectrum obtained without moth eye array. Green line: AM1.5 solar irradiance spectrum. (b) Black line: the difference in the absorption spectra between the cases of applying the optimal moth eye array and not applying moth eye (i.e., the difference in the blue and black lines in (a)). Red line: the difference in the absorption spectra between the cases of applying the moth eye with the smaller period and not applying moth eye (i.e., the difference in the red and black lines in (a)) (Color figure online)

at longer wavelengths in excess of 500 nm, irrespective of whether the moth eye coating is introduced. This will be mainly attributed to the decrease in the extinction coefficient and the increase in the refractive index of P3HT:PCBM at the longer wavelengths (Fig. 2), as discussed in the previous study.[19] In Fig. 6b, we also plotted the increase in the absorbed energy caused by the optimized moth eye array (black line) and by the moth eye with the smaller L value (red line). The comparison between the two lines in Fig. 6b clearly shows that the effect of applying the optimized periodicity on the energy absorption is particularly large at longer wavelength of ~620 nm, which is

slightly smaller than the wavelength corresponding to the optical band gap of P3HT (653 nm). Therefore, although the optimal structure of ARS is determined by the integration of the optical response over a wide range of wavelength (equation 2), the response at the longer wavelength range plays a critical role in deciding the performance obtained by the optimized moth eye period.

In order to investigate the light propagation at this long wavelength range, we plotted in Fig. 7 the spatial distribution of the phase (Figs. 7a and 7b) and amplitude (Figs. 7c and 7d) of the electric field at $\lambda = 626$ nm. When the period of moth eye is smaller
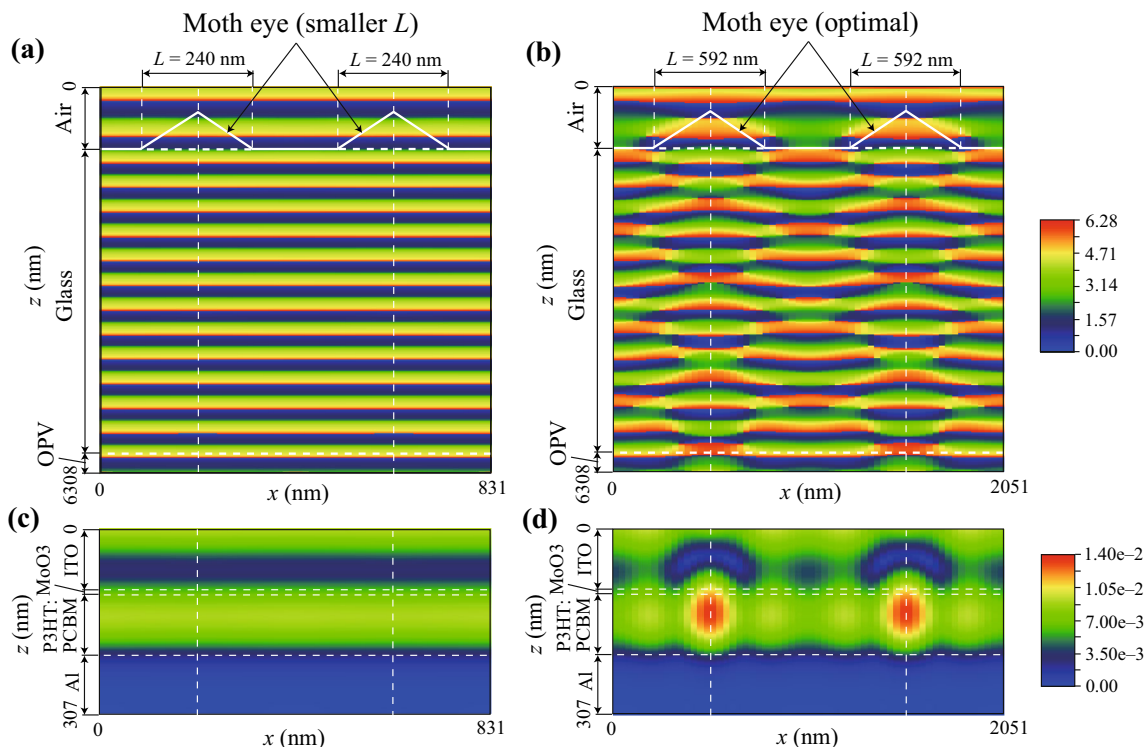
Fig. 7: Spatial distribution of the phase (a, b) and amplitude (c, d) of the electric field in the OPV device with moth eye texture is shown at λ = 626 nm. (a, c) The case of applying the moth eye array with a period smaller than that of the optimal solution (L = 240 nm and H = 601 nm). (b, d) The case of applying the optimized moth eye structure (L = 592 nm and H = 601 nm). In (a–d), the phase or amplitude of the x-component of electric field is plotted as a function of x and z in the plane of y = 0 (see Fig. 1b for the coordinate system). The x-component of electric field is shown here, because the y-component of electric field disappears, due to a spatial symmetry of the model, and the z-component of electric field tends to be much smaller than the x-component, due to the use of the x-polarized incident light (see "Experimental")[16] (Color figure online)

(L = 240 nm), the light passes straightforward through the substrate and OPV cell (Fig. 7a), and therefore, the electric field intensity does not change horizontally (i.e., in the direction perpendicular to the incident light axis) (Fig. 7c). In contrast, in the case that the optimal period of moth eye (L = 592 nm) is used, the light is significantly bent by diffraction (Fig. 7b) and the electric field has strong peak within the active layer (Fig. 7d). This result can be explained by the fact that the diffraction of electromagnetic wave is particularly large when the wavelength nearly agrees with the period of textured surfaces.[41] These results suggest that the optimized moth eye structure with the longer period is effective to bend the light path and strengthen the electric field intensity in the active layer, leading to the enhanced photocurrent generation.

Conclusion

In this study, we explored the optimal moth eye structure to maximize J_{SC} of OPVs. We applied the two-step optimization algorithm, in which the SGS and PS algorithms are used for a rough estimation of the global optimal solution and the refinement of the solution, respectively. We also introduced a computational algorithm to remove the artificial interference effect, which arises in FDTD simulations due to the existence of a thick glass substrate. The optimal moth eye structure was found to have the period of L = 592 nm and the height of H = 601 nm, and increase the level of J_{SC} by 9.05%. Since the period of the optimized moth eye texture is longer than the typically used value (L < 300 nm),[23,39,40] we investigated the reason why the use of such larger value of L can improve the performance. We found that the increase in the absorbed energy by the optimal moth eye structure was particularly large at longer wavelength of ~620 nm, which is slightly below the wavelength corresponding to the band gap of P3HT (653 nm). By analyzing the light propagation at the longer wavelength range, we revealed that the light path is significantly bent by the moth eye with the optimal period (but not with smaller period), which leads to the strengthening of the electric field in the active layer. These results are helpful to allow for a practical optimization design of surface nanostructure for efficient light trapping of OPVs.

Appendix: Method for removing artificial interference effect from FDTD response

This appendix shows the detail of the algorithm to eliminate the artificial interference effect, due to the existence of a thick glass substrate, from FDTD results. The algorithm can be summarized in (1)–(3) as follows:

(1) Let us denote r_i ($i = 1, ..., N$) to be the response r (e.g., absorbance, reflectance, or transmittance) obtained by FDTD simulation at wavelength λ_i, where $\lambda_1 < \lambda_2 < \cdots < \lambda_N$. We assume that the number of wavelength, N, is large enough so that a set of points $P_i(\lambda_i, r_i)$ ($i = 1, ..., N$) in the plane spanned by λ and r can provide a good approximation of the functional shape of $r(\lambda)$. At each wavelength λ_i, we take the average of the response over nearby p (=21) points such that $\tilde{r}_i = \frac{1}{p} \sum_{j=i-(p-1)/2}^{i+(p-1)/2} r_j$. Then, we define $g(\lambda)$ to be a piecewise linear function given by the linear interpolation of the N points $(\lambda_i, \tilde{r}_i)$ for $i = 1, ..., N$ (i.e., $g(\lambda) = \frac{\tilde{r}_{i+1} - \tilde{r}_i}{\lambda_{i+1} - \lambda_i}(\lambda - \lambda_i) + \tilde{r}_i$ for $\lambda_i \leq \lambda \leq \lambda_{i+1}$).

(2) For all i, we define d_i (>0) to be the minimum distance between the point $P_i(\lambda_i, r_i)$ and the curve of the function $g(\lambda)$ in the λ–r plane, and also define l_i to be a value given by $l_i = d_i$ for $r_i \geq \tilde{r}_i$ and $l_i = -d_i$ for $r_i < \tilde{r}_i$. Then, let Γ_+ and Γ_- be a set of integers i for which l_i is locally maximum and minimum, respectively. Hence, $\Gamma_+ = \{i | l_i > l_{i-1}$ and $l_i > l_{i+1}\}$ and $\Gamma_- = \{i | l_i < l_{i-1}$ and $l_i < l_{i+1}\}$.

(3) We define $f_+(\lambda)$ and $f_-(\lambda)$ to be the functions given by the cubic spline interpolation of the points $P_i(\lambda_i, r_i)$ with $i \in \Gamma_+$ and $i \in \Gamma_-$, respectively. Then, the functions $f_+(\lambda)$ and $f_-(\lambda)$ represent the upper and lower envelopes of $r(\lambda)$, respectively. Finally, we obtain the response curve $\bar{r}(\lambda)$, in which the artificial interference effect has been removed, by averaging the two envelopes $\bar{r}(\lambda) = (f_+(\lambda)$ and $f_-(\lambda))/2$.

References

1. Yu, G, Gao, J, Hemmelen, JC, Wudl, F, Heeger, AJ, "Polymer Photovoltaic Cells: Enhanced Efficiencies via a Network of Internal Donor-Acceptor Heterojunctions." *Science*, **270** 1789–1791 (1995)
2. Sariciftci, NS, Smilowitz, L, Heeger, AJ, Wudl, F, "Photoinduced Electron Transfer from a Conducting Polymer to Buckminsterfullerene." *Science*, **258** 1474–1476 (1992)
3. Park, SH, Roy, A, Beaupre, S, Cho, S, Coates, N, Moon, JS, Moses, D, Leclerc, M, Lee, K, Heeger, AJ, "Bulk Heterojunction Solar Cells with Internal Quantum Efficiency Approaching 100%." *Nat. Photonics*, **3** 297–303 (2009)
4. Krebs, FC, Espinosa, N, Hösel, M, Sondergaard, RR, Jorgensen, M, "25th Anniversary Article: Rise to Power—OPV-Based Solar Parks." *Adv. Mater.*, **26** 29–39 (2014)
5. Jorgensen, M, Norrmann, K, Cevorgyan, SA, Tromholt, T, Andreasen, B, Krebs, FC, "Stability of Polymer Solar Cells." *Adv. Mater.*, **24** 580–612 (2012)
6. Niggemann, M, Blasi, B, Gombert, A, Hinsch, A, Hoppe, H, Lalanne, P, Meissner, D, Wittwer, V, "Trapping Light in Organic Plastic Solar Cells with Integrated Diffraction Gratings." *Proc. 17th Eur. Photovoltaic Solar Energy Conf.*, Munich, Germany, 2001
7. Niggemann, M, Riede, M, Gombert, A, Leo, K, "Light Trapping in Organic Solar Cells." *Phys. Status Solidi A*, **205** 2862–2874 (2008)
8. Raman, A, Yu, Z, Fan, S, "Dielectric Nanostructures for Broadband Light Trapping in Organic Solar Cells." *Opt. Express*, **19** 19015–19026 (2011)
9. Macleod, HA, *Thin-Film Optical Filters*, 4th ed. CRC Press, Boca Raton, 2010
10. Boden, SA, Bagnall, DM, "Optimization of Moth-Eye Antireflection Schemes for Silicon Solar Cells." *Prog. Photovolt. Res. Appl.*, **18** 195–203 (2010)
11. Brunner, R, Sandfuchs, O, Pacholski, C, Morhard, C, Spatz, J, "Lessons from Nature: Biomimetic Subwavelength Structures for High-Performance Optics." *Laser Photonics Rev.*, **6** 641–659 (2012)
12. Sun, CH, Jiang, P, Jiang, B, "Broadband Moth-Eye Antireflection Coatings on Silicon." *Appl. Phys. Lett.*, **92** 061112 (2008)
13. Huang, YF, Chattopadhyay, S, "Nanostructure Surface Design for Broadband and Angle-Independent Antireflection." *J. Nanophotonics*, **7** 073594 (2013)
14. Deinega, A, Valuev, I, Potapkin, B, Lozovik, Y, "Minimizing Light Reflection from Dielectric Textured Surfaces." *J. Opt. Soc. Am. A:*, **28** 770–777 (2011)
15. Forberich, K, Dennler, G, Scharber, MC, Hingerl, K, Fromherz, T, Brabec, CJ, "Performance Improvement of Organic Solar Cells with Moth Eye Anti-reflection Coating." *Thin Solid Films*, **516** 7167–7170 (2008)
16. Kubota, S, Kanomata, K, Suzuki, T, Ahmmad, B, Hirose, F, "Hybrid Antireflection Structure with Moth Eye and Multilayer Coating for Organic Photovoltaics." *J. Coat. Technol. Res.*, **12** 37–47 (2015)
17. Taflove, A, Hagness, SC, *Computational Electrodynamics: The Finite-Difference Time-Domain Method*. Artech House Inc., Norwood, 2005
18. Wang, J, Wang, CW, Li, Y, Zhou, F, Liu, WM, "The Structure Optimization Design of the Organic Solar Cells Using the FDTD Method." *Phys. B*, **405** 2061–2064 (2010)
19. Kubota, S, Kanomata, K, Momiyama, K, Suzuki, T, Hirose, F, "Robust Design Method of Multilayer Antireflection Coating for Organic Solar Cells." *IEICE Trans. Electron.*, **E96-C** 604–611 (2013)
20. Persson, NK, Inganas, O, "Organic Tandem Solar Cells—Modeling and Predictions." *Sol. Energy Mater. Sol. Cells*, **90** 3491–3507 (2006)
21. Persson, NK, Inganas, O, "Simulations of Optical Processes in Organic Photovoltaic Devices." In: Sun, SS, Sariciftci, NS (eds.) *Organic Photovoltaics: Mechanisms, Materials, and Devices*, pp. 107–138. CRC Press, Boca Raton, 2005
22. Han, KS, Shin, JH, Yoon, WY, Lee, H, "Enhanced Performance of Solar Cells with Anti-reflection Layer Fabricated

by Nano-imprint Lithography." *Sol. Energy Mater. Sol. Cells*, **95** 288–291 (2011)

23. Jiao, F, Huang, Q, Ren, W, Zhou, W, Qi, F, Zheng, Y, Xie, J, "Enhanced Performance for Solar Cells with Moth-Eye Structure Fabricated by UV Nanoimprint Lithography." *Microelectron. Eng.*, **103** 126–130 (2013)

24. Boltasseva, A, "Plasmonic Components Fabrication via Nanoimprint." *J. Opt. A*, **11** 114001 (2009)

25. Brigo, L, Mattei, G, Michieli, N, Brusatin, G, "2D Photonic Gratings from Thermal Imprinting of ITO-Based Films." *Microelectron. Eng.*, **97** 193–196 (2012)

26. Lü, C, Yang, B, "High Refractive Index Organic-Inorganic Nanocomposites: Design, Synthesis and Application." *J. Mater. Chem.*, **19** 2884–2901 (2009)

27. Ren, W, Zhang, G, Wu, Y, Ding, H, Shen, Q, Zhang, K, Li, J, Pan, N, Wang, X, "Broadband Absorption Enhancement Achieved by Optical Layer Mediated Plasmonic Solar Cell." *Opt. Express*, **19** 26536–26550 (2011)

28. ASTM G173-03, *Standard Tables for Reference Solar Spectral Irradiances*. ASTM International, West Conshohocken, PA, 2005

29. Darkwi, AY, Lote, WK, Ibrahim, K, "Computer Simulation of Collection Efficiency of a-Si : H Tandem Solar Cells Interconnected by Transparent Conductive Oxide." *Sol. Energy Mater. Sol. Cells*, **60** 1–9 (2000)

30. Luk, WC, Yeung, KM, Tam, KC, Ng, KL, Kwok, KC, Kwong, CY, Ng, AMC, Djurisic, AB, "Enhanced Conversion Efficacy of Polymeric Photovoltaic Cell by Nanostructured Antireflection Coating." *Org. Electron.*, **12** 557–561 (2011)

31. Hoppe, H, Sariciftci, NS, Meissner, D, "Optical Constants of Conjugated Polymer/Fullerene Based Bulk-Heterojunction Organic Solar Cells." *Mol. Cryst. Liq. Cryst.*, **385** 113–119 (2002)

32. Rakic, AD, Djurisic, AB, Elazar, JM, Majewski, ML, "Optical Properties of Metallic Films for Vertical-Cavity Optoelectronic Devices." *Appl. Opt.*, **37** 5271–5283 (1998)

33. Aspnes, DE, "Optical Properties of Thin Films." *Thin Solid Films*, **89** 249–262 (1982)

34. Dixon, LCW, *Nonlinear Optimization*. The English Universities Press, London, 1972

35. Momma, M, Bennett, KP, *A Pattern Search Method for Model Selection of Support Vector Regression*. Proc. SIAM Conf, Data Mining, Philadelphia, 2012

36. Hooke, R, Jeeves, TA, "Direct Search Solution of Numerical and Statistical Problems." *J. Assoc. Comput. Mach.*, **8** 212–229 (1961)

37. Khambampati, AK, Ijaz, UZ, Lee, JS, Kim, S, Kim, KY, "Phase Boundary Estimation in Electrical Impedance Tomography Using the Hooke and Jeeves Pattern Search Method." *Meas. Sci. Technol.*, **21** 035501 (2010)

38. Kubota, S, Kanomata, K, Ahmmad, B, Mizuno, J, Hirose, F, "FDTD Analysis for Light Passing Through Glass Substrate and Its Application to Organic Photovoltaics with Moth Eye Antireflection Coating" (in preparation)

39. Raut, HK, Dinachali, SS, He, AY, Ganesh, VA, Saifullah, MSM, Law, J, Ramakrishna, S, "Robust and Durable Polyhedral Oligomeric Silsesquioxane-Based Anti-reflective Nanostructures with Broadband Quasi-omnidirectional Properties." *Energy Environ. Sci.*, **6** 1929–1937 (2013)

40. Tommila, J, Aho, A, Tukiainen, A, Polojärvi, V, Salmi, J, Niemi, T, Guina, M, "Moth-Eye Antireflection Coating Fabricated by Nanoimprint Lithography on 1 eV Dilute Nitride Solar Cell." *Prog. Photovolt. Res. Appl.*, **21** 1158–1162 (2013)

41. Born, M, Wolf, E, *Principles of Optics*, 7th ed. Cambridge University Press, Cambridge, 1999